ACS APPLIED POLYMER MATERIALS

Article

Cite This: ACS Appl. Polym. Mater. XXXX, XXX, XXX−XXX

pubs.acs.org/acsapm

Anti-Fouling Electroconductive Forward Osmosis Membranes: Electrochemical and Chemical Properties

Perla Cruz-Tato,[†] Nicole Rivera-Fuentes,[†] Michael Flynn,[‡] and Eduardo Nicolau*[,†,§]

[†]Chemistry Department, University of Puerto Rico, Rio Piedras Campus, PO Box 23346, San Juan, Puerto Rico 00931-3346, United States

[‡]Bioengineering Branch, NASA Ames Research Center, Moffett Field, California 94035, United States

Supporting Information

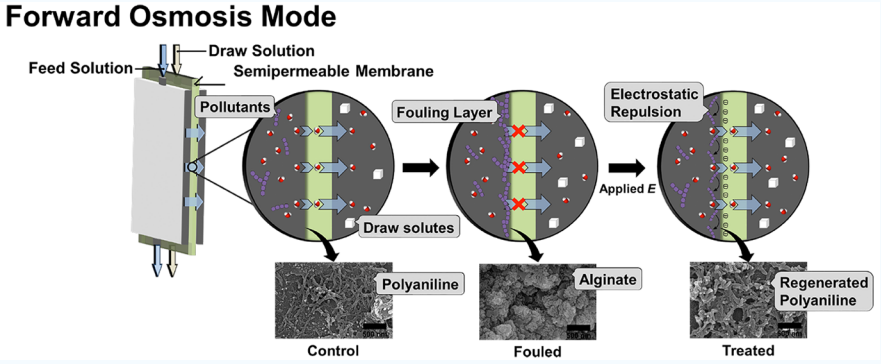

ABSTRACT: Forward osmosis (FO) has been emerging and gaining attention within the membrane-based processes because it can achieve high water fluxes while minimizing energy consumption, making it a cost-effective approach for wastewater treatment. However, membrane fouling remains an obstacle to this application. To address this concern, we fabricated an electroconductive membrane composed of polysulfone and polyaniline (PAni). These membranes have the potential to oxidize targeted organic compounds and/or electrostatically remove the fouling layer. After optimizing the PAni loading, we performed bench-scale tests using sodium alginate as model foulant. The membranes were fouled resulting in a decrease in FO efficiency of 72%. Fouled membranes were treated with a cathodic potential for 30 min, the fouling and antifouling processes were monitored with scanning electron microscopy (SEM), and contact angle and electrochemical methods were used. The fouled membrane exhibited a clogged surface and high electrical resistance, while the treated membrane recovered the PAni nanofibers morphology, its electrical and hydrophilic properties, and 84% of its FO efficiency. Thus, PAni can improve the overall membrane permeability while incorporating antifouling properties. Moreover, the EIS results of this study shed light on the mechanisms that govern the water separation process before and after fouling in the FO mode.

KEYWORDS: *polyaniline, forward osmosis, wastewater reclamation, fouling, electroconductive membrane, electrochemical impedance*

INTRODUCTION

Among membrane-based processes, osmotically driven processes, such as forward osmosis (FO), have attracted researchers, mainly due to advantages related to power consumption as opposed to reverse osmosis (RO), a power-intensive process. FO has been widely studied for different applications, such as wastewater reclamation, desalination, power regeneration, among others.[1] FO is a natural phenomenon that occurs spontaneously when two solutions of different osmotic potentials are separated by a semipermeable membrane. Specifically, it creates an osmotic potential difference ($\Delta\pi$) that makes the water molecules cross the membrane from the feed solution (FS, the solution with lower osmotic potential) to the draw solution (DS, the solution with higher osmotic potential), Scheme 1a.[2,3] Moreover, with the advent of new osmotic agents,[4,5] the FO process has gained track, but research in the area of electrochemically active FO membranes is still limited.

In fact, a common problem associated with wastewater treatment using membrane-based systems is the fouling phenomenon (Scheme 1b). Fouling occurs after prolonged usage of the membrane, where pollutants block the pores and form a film that decreases its overall performance significantly,[6,7] leading to increased operational costs[8,9] and a shortened membrane functional life.[10] When compared to pressure-driven membrane processes, such as RO, FO benefits mainly from (a) lower fouling propensity due to low transmembrane pressure, (b) spontaneous process, (c) high water fluxes and selectivity, and (d) cost-effectiveness. Albeit

Received: January 30, 2019
Accepted: April 16, 2019
Published: April 16, 2019

DOI: 10.1021/acsapm.9b00087
ACS Appl. Polym. Mater. XXXX, XXX, XXX−XXX

Scheme 1. Representation of (a) FO Process and (b) Membrane Fouling after FO Experiment

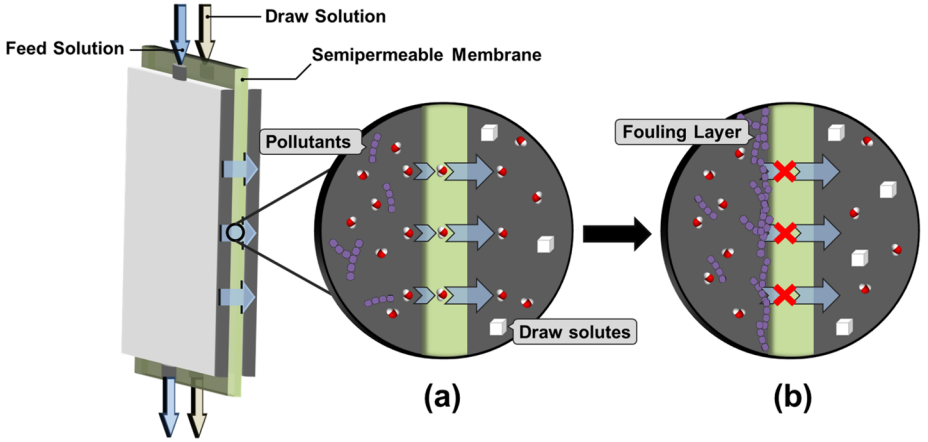

FO exhibits lower membrane fouling, further use and implementation of this technology is still hindered from such effects. The way fouling in FO occurs is quite unique due to the low pressure being applied, which ultimately affects the density of the resulting fouling layer.[11,12]

Common fouling agents found in wastewater, such as polysaccharides, are often negatively charged, which makes them prone to electrostatic repulsion by a negatively charged surface.[13] Thus, the fabrication of conductive membranes has emerged as a sound strategy to mitigate the fouling of the membrane.[14] The electroconductive reactive membranes are a key advancement in the area of water purification, as they prevent or remove the fouling layer that is typically removed by chemical and mechanical means. This process is achieved by two possible mechanisms, (1) electrostatic repulsions or (2) electrochemical reactions (e.g., oxidation of certain contaminants). Both mechanisms work as a response to an applied electric pulse through the membrane that occurs in situ. Although the area of electroconductive reactive membranes is still in development, researchers have explored the incorporation of metal nanoparticles,[15] carbonaceous species,[16] metallic scaffolds,[17] and less common, electrically conductive polymers (ECPs).[18] Among the ECPs, polyaniline (PAni) is one of the most extensively studied due to its low production cost, simple synthesis, mechanical and environmental stability, and adjustable conductivity.[19] PAni exhibits high conductivity in its partially oxidized state and good chemical reversibility.[20] PAni exists in several forms (Scheme S1), depending on the potential applied, and assumes distinctive properties, depending on the oxidation or protonation degree. It has been shown, that PAni nanostructures (e.g., fibers) assemble into highly porous, hydrophilic, and high surface area electrodes.[21]

In light of all these facts, herein we explore the incorporation of PAni into a polysulfone (PSF) support in order to shed light on the mechanisms that govern the water separation process before and after fouling. This work provides a thorough study on the fabrication essentials of the electroconductive reactive membranes and how fouled membranes can be reconstituted by employing electrical pulses. More importantly, this is one of the few works in the literature that provides a chemical and electrochemical focus to understand the fouling layer formation and removal processes in the FO mode.

EXPERIMENTAL SECTION

Materials. PSF (average $M_n \sim 22\,000$), *N*-methyl-2-pyrrolidone (NMP, 99%), aniline (ACS reagent, 99.5%), hydrochloric acid (HCl, 37%), ammonium persulfate (APS, ACS reagent 98%), potassium chloride (KCl, ACS reagent 99%), potassium ferrocyanide trihydrate (ACS reagent, 99%), potassium ferricyanide (ACS reagent, 99%), sodium chloride (NaCl, ACS reagent 99.0%), and sodium alginate (SA) were purchased from Sigma-Aldrich. The reagents were used as received; i.e., no further purification was carried out. Nanopure water (18.2 MΩ·cm^2) was used at all times.

PSF Support Fabrication. The membranes were prepared using the nonsolvent-induced phase separation (NIPS) process in accordance with the methodology described in our previous publication.[22] Briefly, a 12% w/v PSF dope solution was prepared in NMP, stirred overnight at room temperature for complete dissolution, and casted over a polyester (PE) mesh (105 μm, 52% open area from Elko Filtering Co.) attached to a clean glass plate. The film thickness was controlled with a doctor blade casting knife and adjusted to 150 μm. Thereafter, we immersed it in a DI water precipitation bath for 10 min before transferring the membrane to a DI water bath for storage.

Polymerization of Aniline. The PSF:PAni membranes were fabricated through a chemical oxidative polymerization (COP) reaction. In brief, the PSF support was immersed and stirred for 24 h in 0.2 M aniline in 0.5 M HCl solution. Then, a solution of 0.05 mM of APS was added dropwise and was allowed to react for 48 h. The membranes were rinsed several times and stored in DI water.

Membrane Characterization. Infrared spectra of air-dried samples were recorded on a Bruker Alpha Platinum-ATR Spectrometer using transmittance mode. A small piece of the membrane was analyzed, and the spectral width ranged from 600 to 4000 cm^{-1}, with 4 cm^{-1} resolution and an accumulation of 64 scans. The electrochemical measurements were performed using a Biologic SP-240 potentiostat from Biologic USA and a custom-made 3-electrode cell, where the membrane was used as the working electrode on a fluorine-doped tin oxide (FTO) and carbon tape contact, the reference electrode was Ag/AgCl (0.197 vs NHE), and the counter electrode was a platinum wire. A Hitachi S-4800 field emission scanning electron microscope (SEM) was used with an accelerating voltage of 10.0KV and a current of 5 μA to analyze the morphology of the membrane's surface. Air-dried samples were fixed onto a sample holder and sputtered with a gold−palladium film (ca. 5 nm thick). Contact angle measurements were carried out using a Theta Lite Optical Tensiometer (Biolin scientific, Gothenburg, Sweden) at room temperature. A 1 cm^2 coupon of each air-dried membrane was fixed, and a 3.0 μL DI water droplet was used for the analysis. The tensiometer records drop images as a function of time and analyses the drop shapes using OneAttension software (Version 1.5).

The permeability performance was tested using a custom-made flow-cell with deionized water (18 MΩ·cm^2) as the feed solution (FS)

DOI: 10.1021/acsapm.9b00087
ACS Appl. Polym. Mater. XXXX, XXX, XXX−XXX

and an aqueous 5% w/v NaCl solution as the draw solution (DS). The exposed area of the membrane was 4.25 cm^2, the active layer was facing the feed solution, and the results were collected at a constant flow rate of 12.3 mL/min and constant temperature of 22 ± 1°C for one hour. The water fluxes, J_w in LMH ($L{\cdot}m^{-2}{\cdot}h^{-1}$), were calculated using the following equation

$$J_w = \frac{\Delta V}{A_M t} \quad (1)$$

where ΔV is the volume increment in the draw solution in L, A_M is active membrane area, and t is time or duration of test in hours.

The reverse salt flux, J_s in GMH ($g{\cdot}m^{-2}{\cdot}h^{-1}$), from the draw solution to the feed solution was calculated using eq 2

$$J_s = \frac{\Delta(C_t V_t)}{A_M t} \quad (2)$$

where C_t and V_t are the salt concentration and the feed volume at the end of the FO experiments, respectively. In order to determine the salt concentration in the feed solution, we measured the solution conductivity and used a calibration curve of NaCl solutions (i.e., concentration−conductivity).

Fouling Experiments. To simulate the fouling of the membranes, SA was used as model foulant. The fouling experiment was carried out in the FO mode, using the same setup conditions as the FO performance, for 8 h with concentrated solutions. A 2000 ppm of SA was used as the feed solution and 3 M NaCl as the draw solution; a concentrated draw solution was used to maintain the osmotic gradient and promote the water flux from the FS to the DS. Thereafter, the FS and DS were changed to DI water and 5% NaCl, respectively, and these fluxes were compared to the unfouled (i.e., control) membrane.

PAni Electrical Regeneration. To remove the fouling layer and regenerate the PAni electroconductive reactive layer, an electric pulse of −2 V vs Ag/AgCl was applied for 30 min in 0.1 M KCl/0.5 M HCl, where the HCl promotes the protonation of the PAni, and the KCl maintains the electroneutrality of the system. The experimental setup is shown in Scheme S2. The regeneration process was monitored by cyclic voltammetry (CV), electrochemical impedance spectroscopy (EIS), SEM, contact angle, and FO water flux experiments and compared to the control membranes. Table 1 summarizes the experimental conditions employed for the electrochemical studies.

Table 1. Summary of Electrochemical Experiments To Monitor the Formation of the Fouling Layer and the Regeneration of the PAni Layer[a]

	technique	solution	experimental conditions
1	CV	Ferric/Ferrous	−1 to 1.5 V at 25 mV/s for 3 cycles
2	EIS	Ferric/Ferrous	E_{oc} = 0 V; voltage amplitude, 20 mV; frequency range, 0.5 MHz to 5.0 Hz and 10 points per decade
3	CV	HCl/KCl	−2 to 2 V at 100 mV/s for 3 cycles

[a]All experiments were carried using a custom-made 3-electrode cell where Ag/AgCl was used as a reference electrode and a Pt wire as the auxiliary electrode. The solutions used were 5 mM Ferric/Ferrous in 0.1M KCl and 0.5M HCl in 0.1M KCl.

RESULTS AND DISCUSSION

PSF:PAni Membrane. PAni is an intrinsic conductive polymer with high hydrophilicity, deposited over a PSF support through a COP reaction. Previous reports have established that the type of dopant used during the COP influences the electrical conductivity of PAni composites, where higher conductivities are achieved using strong protonic acids, such as hydrochloric acid as a dopant.[23] In this work, due to the high porosity of the PSF, the PAni monomers are likely adsorbed to the surface, although some permeate through the pores. After the addition of the oxidant solution, the aniline monomer polymerized within the PSF support and showed a significant change in color from white to green. Figure 1a shows the optical images of the bare PSF support and the PSF:PAni membrane, where the final membrane exhibits an intense green color suggesting the deposition of the conductive polymer.[24] This conductive polymer is color specific (Scheme S1), and each color provides a visual corroboration of the deposited PAni form. The green color observed in the deposited layer (Figure 1b) suggests that the PAni form deposited is the emeraldine salt (ES). To confirm the chemical integrity of the membrane, FTIR was employed. Figure 1c shows the FTIR spectra of the studied materials, where the typical feature of PSF[25] and PAni[23] are observed. The PSF:PAni spectra exhibit similar vibration bands with the PSF support at lower wavenumbers, where the sulfones show very strong absorption bands at these energies. Most of the PAni absorption bands are overlapped with PSF bands since both polymeric structures have benzene and similar vibration energies. However, corresponding to the vibration energy to the secondary aromatic amine in PAni, the N−H stretches of ∼3250 and 3040 cm^{-1} (vw bands) are observed in the PSF:PAni.

The deposition of PAni over the PSF support was validated by the physical change and the presence of new vibration bands in the composite Fourier-transform infrared spectra (FTIR). Nevertheless, the main purpose of adding this polymer to the PSF support was to incorporate functionalities that could render a conductive membrane. CV was used to corroborate the incorporation of such features (i.e., conductivity). A comparison of the CV between the fabricated membranes under the same experimental conditions is shown in Figure 2. At the studied potential window (−2 to 2 V vs Ag/AgCl), PSF (inset graph in Figure 2a) did not exhibit any electrochemical activity, although water oxidation and hydrogen evolution were observed at 2 V and −2 V vs Ag/AgCl, respectively. Furthermore, the voltammogram of PSF:PAni shows the characteristic electrochemical behavior of PAni in HCl, showing that the polymeric layer is electrochemically active. Using this voltammogram, the chemical structure of the deposited PAni can be corroborated.[24] In the anodic sweep, a $-2H^+$ oxidation takes place, from ES to pernigraniline salt at 0.9 and 1.7 V vs Ag/AgCl. In the cathodic sweep, the opposite reaction occurs. The first protonation (H^+) occurs at −0.04 V vs Ag/AgCl, and the second protonation is observed at −0.6 V vs Ag/AgCl. These transitions can also be validated by the visual change in color at the membrane's surface.

Previous works have suggested the importance of PAni loading and how it influences essential properties of the membrane, such as hydrophilicity, roughness, porosity, and conductivity.[26] Thus, in this work, the PAni loading at the PSF support was carefully optimized. Different loadings of PAni per membrane area (2.6, 8.8, and 24.8 mL/cm^2) were tested and were further scrutinized by means of morphological changes, contact angle, electrochemical properties, and FO performance.

The morphology of the active side of the fabricated PSF:PAni membranes was studied using SEM micrographs. Figure 3a,b shows the PSF support (0.0 mL/cm^2 ratio) prior to modifications, where a smooth surface with pores in the range of ca. <100 nm can be observed. Figure 3c−h shows the SEM

DOI: 10.1021/acsapm.9b00087
ACS Appl. Polym. Mater. XXXX, XXX, XXX−XXX

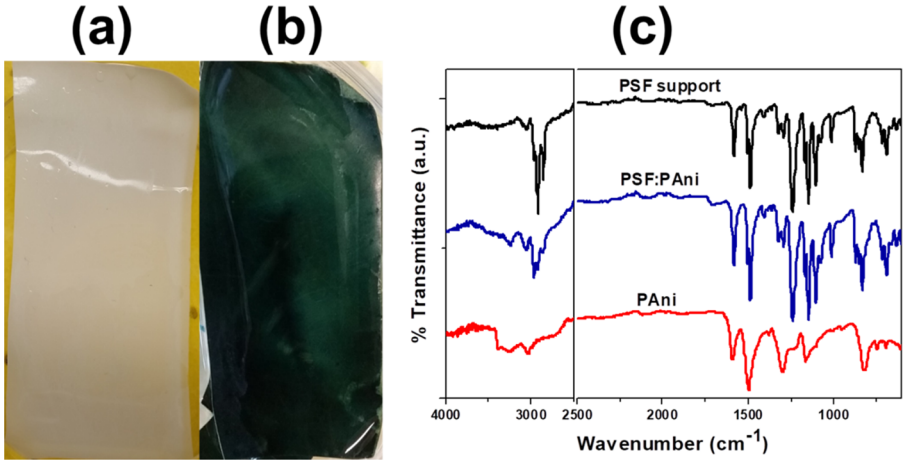

Figure 1. Optical images of fabricated PSF-based membranes. (a) PSF support, (b) PSF:PAni composite membrane after polymerization, and (c) FTIR spectra of individual and combined materials.

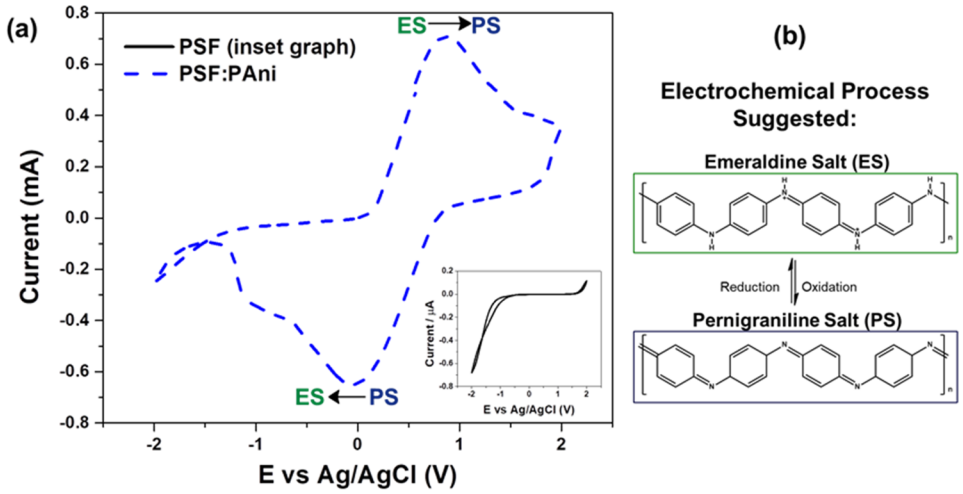

Figure 2. PSF-based membrane (a) CVs of PSF membrane (inset graph) and PSF−PAni for electrochemical property evaluations in a 3-electrode cell setup, at 10 mV/s in 0.5 M HCl/0.1 M KCl. Reference electrode is a Ag/AgCl (NaCl satd, 0.198 V vs NHE) and a platinum wire as a counter electrode. (b) Suggested electrochemical process and optical images at the respective potentials.

micrographs of the PSF:PAni fabricated with different PAni ratios. At the 2.6 mL/cm^2 ratio (Figure 3c,d), the PAni appears in short nanofibers with some disconnected nanoparticles. As the ratio increases, the PAni nanofibers become longer and abundant at the PSF support. When the 8.8 mL/cm^2 ratio is reached (Figure 3e,f), a larger PAni network is observed, while at a higher ratio, 24.8 mL/cm (Figure 3g,h), a denser morphology is obtained with poorly defined fibers.

Thereafter, the electrochemical properties of the different PAni membranes were studied using CV in the presence of a common redox mediator $[Fe(CN)_6]^{3-/4}$ (Ferric/Ferrous). The studies reported in Figure S1 were conducted in potassium chloride at a potential range of −1.0 to 1.5 V vs Ag/AgCl. In the experiment, the membrane's CV was evaluated as a function of scan rate (Figure S1a), where it exhibited a well-defined oxidation and reduction peak of the redox mediator, which validates the membrane's electroactivity and chemical reversibility. Faster scan rates lead to higher currents due to a decrease in the diffusion layer at the membrane's surface.[27] Each peak current (i_p), anodic and cathodic, was found to be almost directly and inversely proportional with the square root of the scan rate, respectively, and this behavior suggests a quasi-reversible redox process. To study the kinetics, the Randles−Sevcik eq (eq 3) can be employed to determine the experimental diffusion coefficient

$$i_p = 2.687 \times 10^5 n^{3/2} A D^{1/2} C^0 \nu^{1/2} \quad (3)$$

where n is the number of electrons in the half-reaction of the redox probe (n = 1), A is the electrode's geometric area, D is the diffusion coefficient, C is the bulk concentration, and ν is the scan rate. The diffusion coefficient of electroactive species, from the bulk solution to the electrode's surface, will depend on the electrode's shape, size, and material.[28,29] In this work, all three membranes are made of the same material; however, as shown in the SEM, the shape and the size of the conductive material vary among them. The 8.8 mL/cm^2 ratio has the highest diffusion coefficient and slope at the $i_p/\nu^{1/2}$, suggesting that the redox probe diffuses freely and faster within the polymeric layer (see the Supporting Information, Figure S2). Interestingly, the highest PAni ratio deposited (24.8) was the least electrochemically efficient in terms of the kinetics as well as in the proportionality between the $i_p/\nu^{1/2}$. Previous reports account for the fact that PAni nanofibers have a higher surface area that facilitates rapid ion exchange.[30−32] Thus, the obtained

DOI: 10.1021/acsapm.9b00087
ACS Appl. Polym. Mater. XXXX, XXX, XXX−XXX

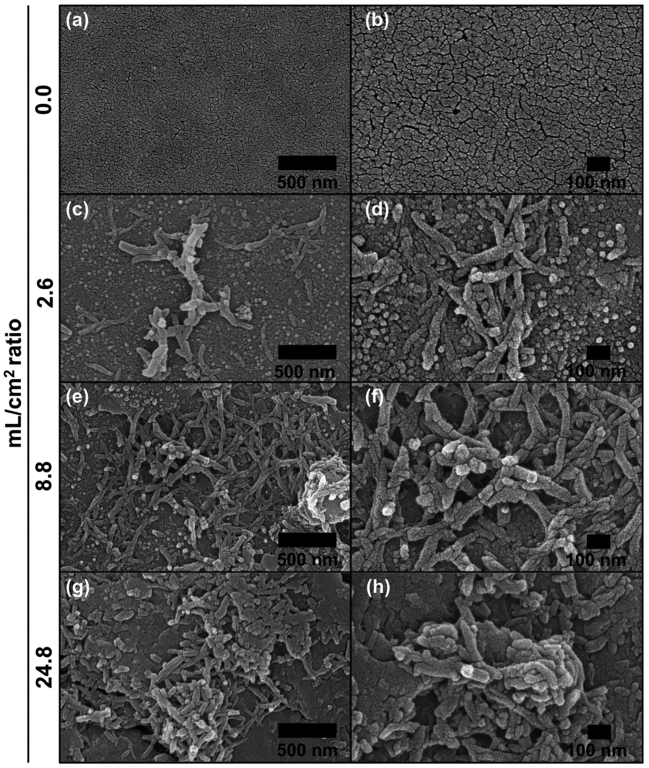

Figure 3. SEM micrographs of the (a, b) PSF support and the studied PAni ratios (mL/cm^2) in the PSF:PAni composite membranes, (c, d) 2.6, (e, f) 8.8, and (g, h) 24.8, at different magnifications 50× and 100×.

trend in this study can be correlated with the SEM images, where the more defined and abundant PAni fibers are obtained at the 8.8 ratio. The 24.8 ratio has a denser PAni layer, which could lead to a larger diffusion layer and therefore a lower measurable faradaic current.

Further, the wettability of each membrane was measured by contact angle (CA) after 10 s of DI permeation, and the results are summarized in Table 2. All membranes have a CA smaller

Table 2. Comparison of the Studied PAni Ratios (mL/cm^2) in the PSF:PAni Composite Membrane[a]

		PAni Ratios (mL/cm^2)			
		0.0	2.6	8.8	24.8
(a)	Contact Angle, Θ (degrees ± SD)	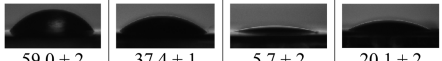 59.0 ± 2	37.4 ± 1	5.7 ± 2	20.1 ± 2
(b)	Water Flux, J_w (LMH ± SD)	8.4 ± 1	1.7 ± 0.6	12.7 ± 0.9	3.1 ± 0.9

[a](a) Contact angle measurements and (b) water fluxes.

than 90°, which indicates all are hydrophilic in nature. When compared among them, the PSF support (0.0 mL/cm^2 ratio) is the most hydrophobic, followed by the 2.6, 24.8, and 8.8 ratio; within these results, we did not observe a direct proportionality with the PAni ratio.

The FO performance of each membrane results, in Figure 4, show that the membrane with the 8.8 mL/cm^2 PAni ratio reached the highest water flux, 12.7 LMH, which represents an increment of 34% over the PSF support. In contrast, the 2.6 and 24.8 mL/cm^2 ratios exhibited lower water fluxes than the

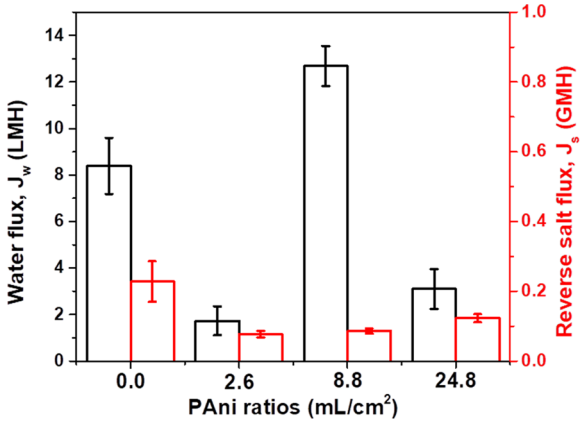

Figure 4. Water flux and reverse salt flux performance of the fabricated PSF:PAni membranes. Experiments were run for 1 h using DI water as the feed and 5% w/v NaCl as the draw solution.

PSF support. On the other hand, the reverse salt flux of all PSF:PAni membranes is lower than the PSF support, and this suggests that the addition of a cross-linked layer to the support surface prevents the salt ions from migrating to the feed solution. Interestingly, the lowest J_s was also obtained with the 8.8 ratio.

Overall, the PSF support does not exhibit any electroactivity and has a homogeneous hydrophobic surface that allows for proper water permeability. Modification of this support with 2.6 mL/cm^2 PAni makes the membrane 37% more hydrophilic; however, the J_w decreases significantly (i.e., 80%). Similarly when the support is modified with 24.8 mL/cm^2 PAni, the membrane hydrophilicity increases up to 66%, but the water permeability decreases by 63% before the modification. In contrast, when the 8.8 mL/cm^2 PAni ratio is used, the membrane becomes very hydrophilic (90%), which allows for higher water permeability (34%). These results indicate that the optimal PAni ratio is 8.8 mL/cm^2, and for the purposes of investigating the chemical and electrochemical intricacies of these membranes, it provides a suitable case study. The 8.8 mL/cm^2 PAni ratio was found to be optimal because it exhibits (1) well-dispersed nanofibers, (2) the highest diffusion coefficient, (3) the most hydrophilic surface, (4) the highest water flux, and (5) the lowest reverse salt flux.

Fouling and Electrochemical Membrane Regeneration. Membrane fouling is still a drawback to the applications of the FO process for wastewater reclamation. To evaluate the feasibility of using PAni to mitigate this issue and to understand its fundamental mechanism, we performed bench-scale tests. First, the studied membranes, PSF and PSF:PAni, were fouled using SA, which has been reported as a typical foulant for carbohydrates.[17] As expected, after an 8-h fouling experiment in the custom-made flow cell, the membrane pores became blocked; consequently, the FO performance of the membranes decreased significantly. Then, the fouled membrane was transferred to the electrochemical cell (Scheme S2), where a cathodic voltage (i.e., an electric pulse of −2 V vs Ag/AgCl) was applied for 30 min to strip the fouling layer and regenerate the PAni active layer to recover its efficiency. The cathodic potential was selected to promote the electrostatic repulsion of the alginates and to force the formation of the ES, granting higher water permeability and electroactivity. By applying the potential of −2 V vs Ag/AgCl, we promote that the membrane acts as a cathode, and thus, we

DOI: 10.1021/acsapm.9b00087
ACS Appl. Polym. Mater. XXXX, XXX, XXX−XXX

focus on the reduction reaction at its surface. Even though chlorine gas could potentially form in the studied anode (Pt wire) at the applied potential, it does not exhibit any ionic charge or possible attraction to either the alginate layer or the negatively charged membrane after applying the cathodic potential. Therefore, if any chlorine is formed at the anode or remains in solution, it will not affect the fouling of the membrane.

The fouling and PAni regeneration processes were monitored using physical changes at the membrane surface using SEM and CA. The SEM images in Figure 5a account for the presence of the alginate layer and the regeneration of the PAni nanofibers (similar to that in Figure 3e,f), respectively. On the other hand, the CA results (Figure 5b) suggest the same trend, higher CA values are reached when the membrane is fouled due to the presence of a more hydrophobic material and the reduction of the membrane pores. After the cathodic potential treatment, the CA was reduced 60%, suggesting the regeneration of the hydrophilic PAni structure. Experiments without applying voltage were also conducted (data not shown). We observed that PAni structures were slightly more present than in the fouled membrane. We verified this with SEM, where few PAni fibers are present within the fouling layer, and interestingly, some potassium chloride seemed to be deposited over it. The contact angles of these membranes decreased when compared to the fouled membrane, but they were still higher than those of the treated membrane. The same trend was observed in the water flux.

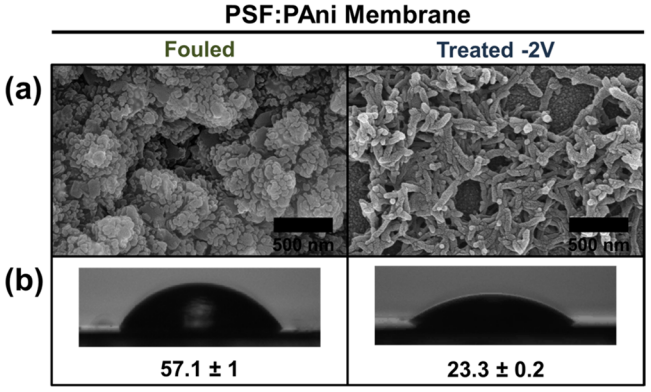

Figure 5. PSF:PAni membrane physical comparison between the fouled and treated stages. (a) SEM micrographs and (b) contact angle measurements.

Electrochemical measurements were also used to study the fouling and the PAni regeneration processes, specifically CV and EIS (Figure 6). EIS is a nondestructive and sensitive method that can be used to analyze the structural characteristics and changes on a surface, such as a porous membrane. This technique provides information about the electrical properties of multilayered systems (i.e., membrane and electrolyte).[33,34] EIS is regularly utilized in the area of lipid bilayer membranes.[35,36] Although such systems are different in chemical nature to the that presented in this article, both describe the passive ion permeation through the membrane pores. In order to understand and assign the different RC

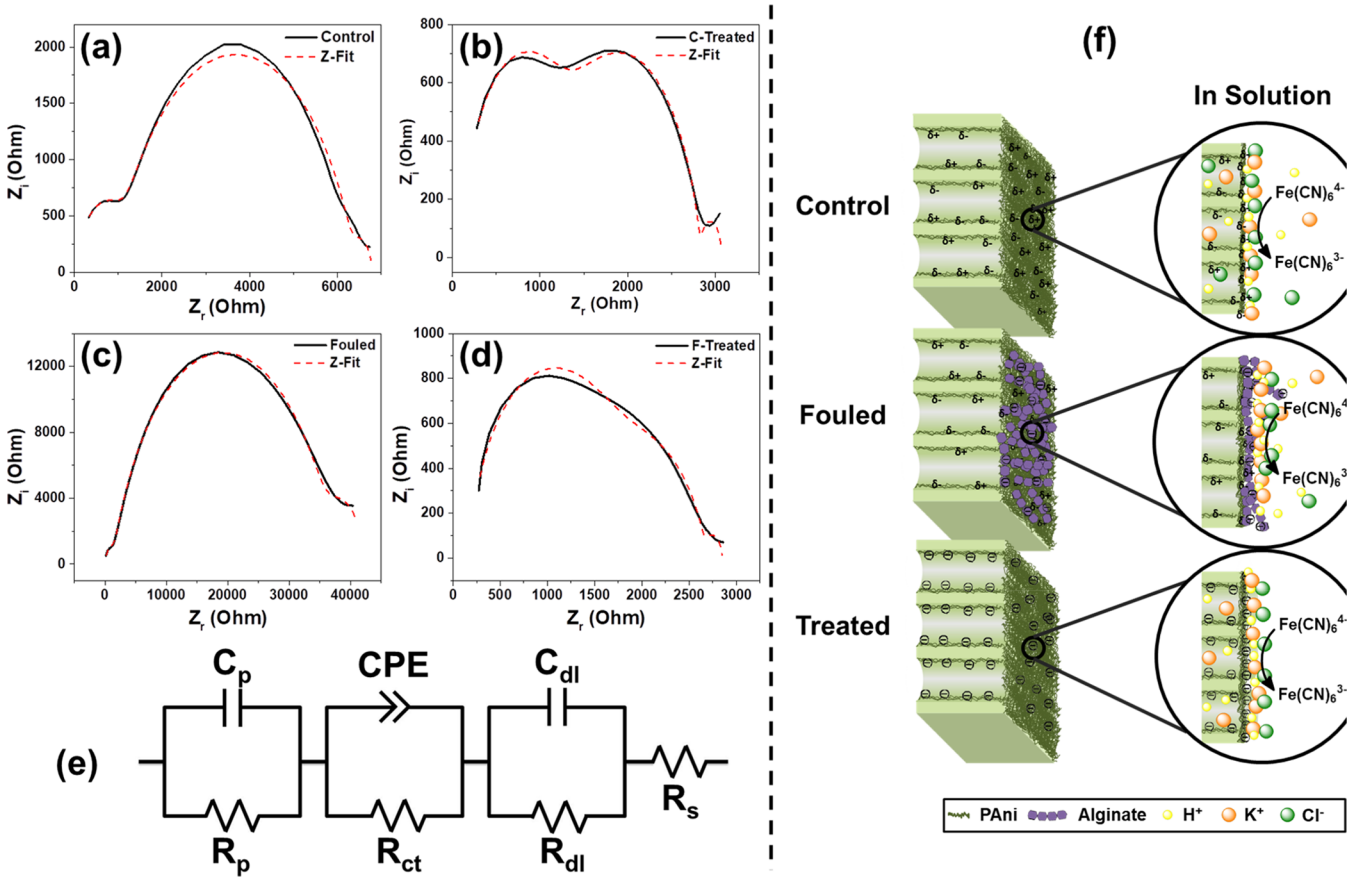

Figure 6. Electrochemical impedance results. (a–d) EIS spectra of each membrane and their respective fitting of the EEC simulation, (e) equivalent electrical circuit, and (f) EIS setup scheme.

DOI: 10.1021/acsapm.9b00087
ACS Appl. Polym. Mater. XXXX, XXX, XXX−XXX

Table 3. Fitting Values for the Equivalent Circuit Elements by the Simulation of EIS

		R_s (Ω)	CPE (nF.s$^{(\alpha-1)}$)	α	R_{ct} (Ω)	C_{dl}, F	R_m (Ω)	C, F	R_p (Ω)	X^2 ($\times 10^{-2}$)
PSF:PAni	control	82.74	69.25	0.785	5425	18.71 μ	385.7	0.611 n	905.3	1.21
	C-treated	120.8	44.33	0.845	1618	0.681n	1102	27.82 μ	232.6	1.95
	fouled	16.54	39.97	0.789	35832	3.13 μ	5098	0.751 n	1207	2.74
	F-treated	192.8	132.7	0.789	1094	0.960n	1394	12.31 μ	166.5	5.69

circuits to the membrane-solution interfaces, we followed reported models with phospholipid membranes, which describe the passive ion permeation using the solubility-diffusion theory. For a better comparison between the control and fouled membrane, we studied four different PSF:PAni membranes, (1) control (i.e., the clean membrane), (2) control membrane treated with the electric pulse (C-treated), (3) fouled membrane and (4) fouled membrane treated with the electric pulse (F-treated). Similar to Sengur-Tasdemir[37] et al., we used the EIS results to model the equivalent electrical circuit (EEC), and then we provided a description and quantitative analysis of the physical properties of the studied system. The Nyquist plots are shown in Figure 6a–d, these results were analyzed with the EC-Lab V10.40 software, and the EECs were chosen to better describe the properties of the membrane and to obtain a suitable model. The circuit elements for the EEC are shown in Figure 6e, and their respective values are reported in Table 3. The selected EEC has 4-elements in series, an individual resistance (R_s) and three RC circuits that correspond to each of the formed interfaces within the system (see scheme in Figure 6f). In the EIS, the beginning of the first semicircle at high frequencies (right to left) is ascribed to the uncompensated bulk resistance (R_s), i.e,. ohmic resistance due to the presence of an electrolyte within the membranes and in solution. It has been shown, that more porous membrane morphology leads to higher R_s,[37] thus the control samples (untreated and treated) showed similar values. In contrast, there is a significant increment from the Fouled membrane, 16.49 Ω, to the F-treated 192.8 Ω, and this suggests that the pores at the F-treated become exposed and unclog after the electrical treatment.

Then, the first RC circuit is attributed to the formation of a double-layer (dl) that arises from the alignment of solvated counterions (i.e., electrolyte) along the membrane's surface. The specific arrangement of the solvated electrolytes is directly dependent on the membrane's electronic distribution and partial charges. Electrically conductive polymers typically have a conjugated backbone formed by a series of altering single and double carbon bonds, and within these π-bonds, the p-orbitals overlap, allowing for the electrons to move freely between atoms. Different dopants can be incorporated to improve the conductivity by introducing a minor charge carrier that removes or adds electrons from/to the polymer chain.[38] In this work, we doped the PAni with HCl, and it is hypothesized that the fabricated PAni could exhibit both types of minor charge carriers (i.e., holes and electrons), which translate into partial $\delta+$ and $\delta-$ charges within the membrane. By the presence of both partial charges, more charges are accumulated at the membrane's surface, and thus, the capacitance (C_{dl}) values are higher by a 10^3 factor at the untreated membranes than at the treated membranes. However, when the R_{dl} values are compared, the fouled membrane has a 13-fold value higher than that of the control one because of the additional alginate layer.

The followed semicircle in the EIS corresponds to the second parallel RC circuit that combines the resistance due to charge transfer (R_{ct}) and a constant phase element (CPE, Q). The CPE was used in the EEC for the simulation of the impedance results as it takes into account the lack of homogeneity (nonideal) of the conductance and the membrane. The impedance of a nonideal electrode is dependent on an α value that describes the deviation from an ideal capacitor. The α values vary from 0 to 1, and $\alpha = 1$ defines an ideal capacitor. All the reported values are higher than 0.7; therefore, the CPE element acts more like a capacitor than a resistor.

We observed a remarkable increase in charge-transfer resistance (R_{ct}) in the fouled membrane due to the negatively charged alginate layer, which retarded electron transfer of the $[Fe(CN)_6]^{3-/4-}$ probe to the PSF:PAni membrane. On the other hand, after the membranes were treated with the electric pulse, the R_{ct} decreased in both the C-treated and F-treated. After the electrical treatment, the surface and inner part of the membranes are being polarized, which promotes the homogenization of the PAni species that predominates at the surface. As shown in Figure 2, the PS form of PAni predominates at more-positive potentials and has higher electronic density than the ES form; therefore, the electron transfer within the $[Fe(CN)_6]^{3-/4-}$ is favorable when the ES species predominates. Additionally, in the F-treated, the reduction in R_{ct} suggests that the alginate layer is either eliminated or reduced in thickness. If we compare the specific values of the treated membranes, 1618 and 1094 Ω, we obtain that C-treated > F-treated. This is likely due to the hydrogen evolution reaction, which can be occurring at the C-treated surface when the cathodic potential is applied (see Figure S3a).

Finally, there is the third RC circuit, which is generated by virtue of having a very porous membrane as the working electrode that allows for the movement, impediment, and accumulation of charges. R_p accounts for the resistance of the membrane pores and C_p for the capacitance within it. Certainly, this RC circuit is related to the previous elements. First, an increment in C_p is observed for the C-treated when compared with the control because of the PAni species at the surface was homogenized; therefore, there are less internal repulsions between the electrolytes and the partial charges of the membrane. As for the fouled membrane, the same trend was observed, and these results suggest (a) the same phenomena as the control membrane, but also that (b) the pores were unclogged, allowing it to retain a higher number of charges within the membrane pores.

CV experiments (Figure S3b) were carried out; a significant decrease in the anodic and cathodic current peaks of the $[Fe(CN)_6]^{3-/4-}$ probe was observed due to the negatively charged alginate, and an increment in both currents was observed after the −2 V was applied. These results clearly indicate that the alginate layer from the fouled membrane was potentially removed, while the PAni ES structure predominates at the surface.

DOI: 10.1021/acsapm.9b00087
ACS Appl. Polym. Mater. XXXX, XXX, XXX−XXX

The physical characterization and the electrochemical results suggest that the PAni structure was regenerated at the membrane's surface and, indirectly, suggest that the pores were unclogged after the cathodic potential treatment. In order to validate that the membrane was able to recover its primary function, i.e., water flux, we conducted bench-scale FO performance tests. Figure 7 shows the J_w comparison at the three studied phases (i.e., control, fouled and treated) of the two membranes, PSF and PSF:PAni.

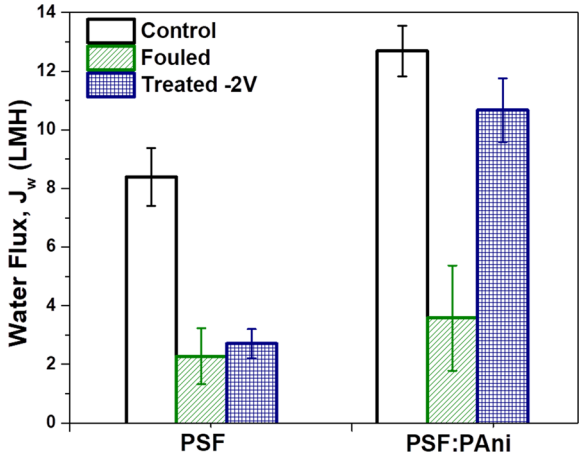

Figure 7. FO performance evaluation of the different membranes, before and after fouling and treatment. Experiments were performed in a custom-made cell for 1 h using DI water as the FS and 5% NaCl aq. as the DS.

First, we calculate the total fouling (F_T) ratio of both membranes using eq 4. After the 8-h experiment, both membranes were clogged in 72%, which only allows for a water flux of 28% when compared to the control. The total fouling ratio was composed of reversible (F_r) and irreversible (F_{ir}) fouling; we use eqs 5 and 6 to calculate their ratios, respectively. In the PSF, only 5% of the total fouling was reversible, and the other 68% of it was irreversible with the applied bias. On the other hand, the fouling on the PSF:PAni was 56% reversible and only 16% irreversible after the applied bias.

$$\%F_T = \left(1 - \frac{J_f}{J_{w,c}}\right) \times 100 \tag{4}$$

$$\%F_r = \left(\frac{J_{w,t} - J_f}{J_{w,c}}\right) \times 100 \tag{5}$$

$$\%F_{ir} = \left(\frac{J_{w,c} - J_{w,t}}{J_{w,c}}\right) \times 100 \tag{6}$$

where J_f is the water flux of the fouled membrane (LMH), $J_{w,c}$ is the water flux of the control membrane (LMH), and $J_{w,t}$ is the water flux of the membrane after the cathodic treatment (LMH).

Finally, we calculate the flux recovery percentage using the following equation

$$\%FR = \frac{J_{w,t}}{J_{w,c}} \times 100 \tag{7}$$

For the PSF membrane, 32% was recovered, while for the PSF:PAni membrane, 84% was recovered. These results are in agreement with the previous characterizations, where we confirm that the membrane pores were clogged with alginate, and after applying an electric pulse, it was removed almost completely when the membrane exhibits conductive properties. Even though the recovery efficiency was not 100%, the obtained water flux was higher than the PSF support by itself.

CONCLUSION

In this work, we were able to incorporate electroconductive properties to the PSF support by adding PAni via chemical oxidative polymerization. The effects of varying the PAni ratio deposited were carefully scrutinized, and the optimal PAni ratio (8.8 mL/cm^2) was selected since it exhibited higher conductivity, hydrophilicity, and permeability Thereafter, we were able to monitor the fouling and antifouling processes by physical changes, wettability, electrochemical properties, and permeability. It was shown that the alginate fouling could be successfully removed by applying a cathodic bias due to electrostatic repulsion, and simultaneously, the PAni layer can be regenerated, which accounted for a recovery in the FO efficiency. Herein, we were able to (1) fabricate electroactive membranes that exhibited promising water fluxes and (2) explore EIS as a powerful analytical tool to examine changes at the membrane's surface produced by fouling and antifouling processes. In future studies, we will study (a) the process with more complex foulants (e.g., calcium) for longer experimental times and (b) the reusability using an in situ setup to improve the membrane properties under operational conditions.

ASSOCIATED CONTENT

Supporting Information

The Supporting Information is available free of charge on the ACS Publications website at DOI: 10.1021/acsapm.9b00087.

Chemical scheme, experimental setup scheme, electrochemical characterizations of the PAni ratios, and electrochemical profile (PDF)

AUTHOR INFORMATION

Corresponding Author

*E-mail: eduardo.nicolau@upr.edu; Phone: 787-292-9820; Fax: 787-522-2150.

ORCID

Eduardo Nicolau: 0000-0002-6116-029X

Present Address

§Molecular Science Research Center, University of Puerto Rico, 1390 Ponce De Leon Ave, Suite 2, San Juan, Puerto Rico 00931-3346, United States

Notes

The authors declare no competing financial interest.

ACKNOWLEDGMENTS

NASA Experimental Program to Stimulate Competitive Research (EPSCoR) under grant #NNX14AN18A and NASA Advanced STEM Training and Research (ASTAR) Fellowship under grant #NNX15AU27H supported this work. The authors acknowledge the NASA Ames Research Center for the provided support during the attainment of this work. We would also like to thank Jin-woo Han and Dong-il Moon for their help with the contact angle measurements. We thank

DOI: 10.1021/acsapm.9b00087
ACS Appl. Polym. Mater. XXXX, XXX, XXX−XXX

the University of California Santa Cruz Materials Analysis for Collaborative Science (UCSC MACS) facility and Joseph Varelas for the access and help with the SEM images. Special thanks to Dr. Edwin Ortíz-Quiles and Dr. Luis Betancourt for helpful discussion and comments on this work. Finally, we give thanks to José Lasalde for designing the schematic representation of the experimental setup.

REFERENCES

(1) Salehi, H.; Shakeri, A.; Rastgar, M. Carboxylic Polyethersulfone: A Novel Ph-Responsive Modifier in Support Layer of Forward Osmosis Membrane. *J. Membr. Sci.* **2018**, *548*, 641−653.
(2) Zhao, S.; Zou, L.; Tang, C. Y.; Mulcahy, D. Recent Developments in Forward Osmosis: Opportunities and Challenges. *J. Membr. Sci.* **2012**, *396*, 1−21.
(3) Sun, Y.; Tian, J.; Zhao, Z.; Shi, W.; Liu, D.; Cui, F. Membrane Fouling of Forward Osmosis (Fo) Membrane for Municipal Wastewater Treatment: A Comparison between Direct Fo and Ombr. *Water Res.* **2016**, *104*, 330−339.
(4) Hartanto, Y.; Zargar, M.; Wang, H.; Jin, B.; Dai, S. Thermoresponsive Acidic Microgels as Functional Draw Agents for Forward Osmosis Desalination. *Environ. Sci. Technol.* **2016**, *50*, 4221−4228.
(5) Chen, Q.; Xu, W.; Ge, Q. Novel Multicharge Hydroacid Complexes That Effectively Remove Heavy Metal Ions from Water in Forward Osmosis Processes. *Environ. Sci. Technol.* **2018**, *52*, 4464−4471.
(6) She, Q.; Wang, R.; Fane, A. G.; Tang, C. Y. Membrane Fouling in Osmotically Driven Membrane Processes: A Review. *J. Membr. Sci.* **2016**, *499*, 201−233.
(7) Bar-Zeev, E.; Perreault, F.; Straub, A. P.; Elimelech, M. Impaired Performance of Pressure-Retarded Osmosis Due to Irreversible Biofouling. *Environ. Sci. Technol.* **2015**, *49*, 13050−13058.
(8) Kwan, S. E.; Bar-Zeev, E.; Elimelech, M. Biofouling in Forward Osmosis and Reverse Osmosis: Measurements and Mechanisms. *J. Membr. Sci.* **2015**, *493*, 703−708.
(9) Radu, A. I.; Vrouwenvelder, J. S.; van Loosdrecht, M. C. M.; Picioreanu, C. Modeling the Effect of Biofilm Formation on Reverse Osmosis Performance: Flux, Feed Channel Pressure Drop and Solute Passage. *J. Membr. Sci.* **2010**, *365*, 1−15.
(10) Luo, W.; Xie, M.; Hai, F. I.; Price, W. E.; Nghiem, L. D. Biodegradation of Cellulose Triacetate and Polyamide Forward Osmosis Membranes in an Activated Sludge Bioreactor: Observations and Implications. *J. Membr. Sci.* **2016**, *510*, 284−292.
(11) Raval, H. D.; Koradiya, P. Direct Fertigation with Brackish Water by a Forward Osmosis System Converting Domestic Reverse Osmosis Module into Forward Osmosis Membrane Element. *Desalin. Water Treat.* **2016**, *57*, 15740−15747.
(12) Chun, Y.; Mulcahy, D.; Zou, L.; Kim, I. S. A Short Review of Membrane Fouling in Forward Osmosis Processes. *Membranes (Basel, Switz.)* **2017**, *7*, 30.
(13) Dudchenko, A. V.; Rolf, J.; Russell, K.; Duan, W.; Jassby, D. Organic Fouling Inhibition on Electrically Conducting Carbon Nanotube−Polyvinyl Alcohol Composite Ultrafiltration Membranes. *J. Membr. Sci.* **2014**, *468*, 1−10.
(14) Ronen, A.; Walker, S. L.; Jassby, D. Electroconductive and Electroresponsive Membranes for Water Treatment. *Rev. Chem. Eng.* **2016**, *32*, 533−550.
(15) Katuri, K. P.; Werner, C. M.; Jimenez-Sandoval, R. J.; Chen, W.; Jeon, S.; Logan, B. E.; Lai, Z.; Amy, G. L.; Saikaly, P. E. A Novel Anaerobic Electrochemical Membrane Bioreactor (Anembr) with Conductive Hollow-Fiber Membrane for Treatment of Low-Organic Strength Solutions. *Environ. Sci. Technol.* **2014**, *48*, 12833−12841.
(16) Ronen, A.; Duan, W.; Wheeldon, I.; Walker, S.; Jassby, D. Microbial Attachment Inhibition through Low-Voltage Electrochemical Reactions on Electrically Conducting Membranes. *Environ. Sci. Technol.* **2015**, *49*, 12741−12750.
(17) Huang, J.; Wang, Z.; Zhang, J.; Zhang, X.; Ma, J.; Wu, Z. A Novel Composite Conductive Microfiltration Membrane and Its Anti-Fouling Performance with an External Electric Field in Membrane Bioreactors. *Sci. Rep.* **2015**, *5*, 9268−9275.
(18) Bogdanovic, U.; Pasti, I.; Ciric-Marjanovic, G.; Mitric, M.; Ahrenkiel, S. P.; Vodnik, V. Interfacial Synthesis of Gold-Polyaniline Nanocomposite and Its Electrocatalytic Application. *ACS Appl. Mater. Interfaces* **2015**, *7*, 28393−28403.
(19) Abu-Thabit, N. Y. Chemical Oxidative Polymerization of Polyaniline: A Practical Approach for Preparation of Smart Conductive Textiles. *J. Chem. Educ.* **2016**, *93*, 1606−1611.
(20) Aggas, J.; Lutkenhaus, J.; Guiseppi-Elie, A. Chemiresistive and Chemicapacitive Devices Formed Via Morphology Control of Electroconductive Bio-Nanocomposites. *Adv. Electron. Mater.* **2018**, *4*, 1700495−1700505.
(21) Huang, J.; Kaner, R. B. The Intrinsic Nanofibrillar Morphology of Polyaniline. *Chem. Commun.* **2006**, *4*, 367−376.
(22) Cruz-Tato, P.; Ortiz-Quiles, E. O.; Vega-Figueroa, K.; Santiago-Martoral, L.; Flynn, M.; Diaz-Vazquez, L. M.; Nicolau, E. Metalized Nanocellulose Composites as a Feasible Material for Membrane Supports: Design and Applications for Water Treatment. *Environ. Sci. Technol.* **2017**, *51*, 4585−4595.
(23) Hu, W.; Chen, S.; Yang, Z.; Liu, L.; Wang, H. Flexible Electrically Conductive Nanocomposite Membrane Based on Bacterial Cellulose and Polyaniline. *J. Phys. Chem. B* **2011**, *115*, 8453−8457.
(24) Shi, Z.; Li, Y.; Chen, X.; Han, H.; Yang, G. Double Network Bacterial Cellulose Hydrogel to Build a Biology-Device Interface. *Nanoscale* **2014**, *6*, 970−977.
(25) Li, J.; Huang, X. J.; Ji, J.; Lan, P.; Vienken, J.; Groth, T.; Xu, Z. K. Covalent Heparin Modification of a Polysulfone Flat Sheet Membrane for Selective Removal of Low-Density Lipoproteins: A Simple and Versatile Method. *Macromol. Biosci.* **2011**, *11*, 1218−1226.
(26) Guillen, G. R.; Farrell, T. P.; Kaner, R. B.; Hoek, E. M. V. Pore-Structure, Hydrophilicity, and Particle Filtration Characteristics of Polyaniline−Polysulfone Ultrafiltration Membranes. *J. Mater. Chem.* **2010**, *20*, 4621.
(27) Elgrishi, N.; Rountree, K. J.; McCarthy, B. D.; Rountree, E. S.; Eisenhart, T. T.; Dempsey, J. L. A Practical Beginner's Guide to Cyclic Voltammetry. *J. Chem. Educ.* **2018**, *95*, 197−206.
(28) Ali, M. A.; Hong, W.; Oren, S.; Wang, Q.; Wang, Y.; Jiang, H.; Dong, L. Tunable Bioelectrodes with Wrinkled-Ridged Graphene Oxide Surfaces for Electrochemical Nitrate Sensors. *RSC Adv.* **2016**, *6*, 67184−67195.
(29) Soni, A.; Pandey, C. M.; Solanki, S.; Sumana, G. One-Pot Synthesis of a Polyaniline-Gold Nanocomposite and Its Enhanced Electrochemical Properties for Biosensing Applications. *RSC Adv.* **2015**, *5*, 45767−45774.
(30) Jeon, J.-W.; Kwon, S. R.; Lutkenhaus, J. L. Polyaniline Nanofiber/Electrochemically Reduced Graphene Oxide Layer-by-Layer Electrodes for Electrochemical Energy Storage. *J. Mater. Chem. A* **2015**, *3*, 3757−3767.
(31) Yan, X.; Tong, X.; Wang, J.; Gong, C.; Zhang, M.; Liang, L. Synthesis of Mesoporous Nio Nanoflake Array and Its Enhanced Electrochemical Performance for Supercapacitor Application. *J. Alloys Compd.* **2014**, *593*, 184−189.
(32) Shabani, P.; Qarehbaqi, A.; Boroumand, F. A. Selective Enhancement of Intra-Chain Charge Transport to Improve Ammonia Sensing Performance in Polyaniline Layers. *Electron. Mater. Lett.* **2016**, *12*, 107−112.
(33) Cen, J.; Kavanagh, J.; Coster, H.; Barton, G. Fouling of Reverse Osmosis Membranes by Cane Molasses Fermentation Wastewater: Detection by Electrical Impedance Spectroscopy Techniques. *Desalin. Water Treat.* **2013**, *51*, 969−975.
(34) Chilcott, T. C.; Cen, J.; Kavanagh, J. M. In Situ Characterization of Compaction, Ionic Barrier and Hydrodynamics of Polyamide Reverse Osmosis Membranes Using Electrical Impedance Spectroscopy. *J. Membr. Sci.* **2015**, *477*, 25−40.

DOI: 10.1021/acsapm.9b00087
ACS Appl. Polym. Mater. XXXX, XXX, XXX−XXX

(35) Valincius, G.; Meškauskas, T.; Ivanauskas, F. Electrochemical Impedance Spectroscopy of Tethered Bilayer Membranes. *Langmuir* **2012**, *28*, 977−990.
(36) Wang, X.; Ma, S.; Su, Y.; Zhang, Y.; Bi, H.; Zhang, L.; Han, X. High Impedance Droplet−Solid Interface Lipid Bilayer Membranes. *Anal. Chem.* **2015**, *87*, 2094−2099.
(37) Sengur-Tasdemir, R.; Guler-Gokce, Z.; Sezai Sarac, A.; Koyuncu, I. Determination of Membrane Protein Fouling by Uv Spectroscopy and Electrochemical Impedance Spectroscopy. *Polym.-Plast. Technol. Eng.* **2018**, *57*, 59−69.
(38) Ahmed, F.; Lalia, B. S.; Kochkodan, V.; Hilal, N.; Hashaikeh, R. Electrically Conductive Polymeric Membranes for Fouling Prevention and Detection: A Review. *Desalination* **2016**, *391*, 1−15.

DOI: 10.1021/acsapm.9b00087
ACS Appl. Polym. Mater. XXXX, XXX, XXX−XXX